Faculty of Natural and Applied Sciences Journal of Scientific Innovations
Print ISSN: 2814-0877 e-ISSN: 2814-0923
www.fnasjournals.com
Volume 5; Issue 1; December 2023; Page No. 34-49.

APPLIED STUDIES OF HETEROCYCLIC AZOMETHINE CHELATOR AND ITS DIVALENT COMPLEXES: SYNTHESIS AND CHARACTERIZATION

***Festus, C., & Didia, L.E.**
Department of Chemistry, Ignatius Ajuru University of Education, Rumuolumeni
PMB 5047, Port Harcourt, Rivers State, Nigeria

***Corresponding author email:** chioma.festus@iaue.edu.ng

Abstract
An azomethine chelator (AC) obtained via condensation of 2-amino-6-nitrobenzothiazole and 2-hydroxy-1-naphthaldehyde was used to formulate M^{2+} complexes. The chelator, and its M^{2+} complexes were characterized using analytical and spectral techniques. AC acquired a yellow solid nature with 77.7% yield and a melting point of 278-280^{o}C. The M^{2+} complexes had different shades, excellent yields and distinct melting points from 206^{o}C. The latter exhibited solubility in dimethylformamide (DMF) and dimethylsurphoxide (DMSO). The infrared spectrum (IR) of AC showed an imine(H-C=N-) band around 1633 cm^{-1} while its M^{2+} complexes had their imine functional group bands between 1616-1642 cm^{-1}. M-N and M-O bonds justifying coordination had their absorption bands appear between 647-513 and 580-457 cm^{-1} respectively. The electronic data of uncoordinated AC, displayed 4-bands at 254, 308, 342 and 398 nm, associated with л→л* and n→π* transitions. Additionally, the M^{2+} complexes showed metal-ligand transition absorptions (428-822 nm) assigned to *d→d* shifts. The corrosion inhibitory investigation of AC at 100, 300 and 500 ppm in 1M-HCl, proved that when the concentration increased, the rate of corrosion consequently decreased while the efficiency of inhibition increased. The presence of S, O_2 and H-C=N, may have aided this activity. *In-vitro* antibacterial screening in DMSO against *S. aureus, B. cerus, P. aeruginosa, P. mirabilis, S. typhi* and *K. pneumoniae* using streptomycin as positive control, presented activities in the range 1.0 – 14.0 mm. *A. niger, A.s flaus,* and *R. stalonfer* were used for antifungal evaluation using miconazole as standard drug. The inhibitions were recorded in the range 1.0–25.0 mm. These results prove that the compounds as promising antibacterial/antifungal drug pro-agents.

Keywords: Heterocyclic, Substituted Azomethine-Based Chelator, Divalent Complexes, Synthesis, Spectral

Introduction

Sequel to IUPAC recommendation, azomethines can be describe as chemical compounds (imines) having a hydrocarbyl specie on the nitrogen atom $R_2C = NR^{III}$ ($R^{III} \neq H$). They are considered by many to be synonymous with Schiff bases (Samaszko-Fiertek et al., 2022). They are versatile ligands formed via primary amines and carbonyl compound condensation reaction, accompanied with the elimination of water molecules (Samaszko-Fiertek et al., 2022). The resultant compound $R^{I}R^{II}C=NR^{III}$ is known as azomethine (often called imine), in which R^{I} represents aryl specie, R^{II} stands for hydrogen atom and R^{III} represents aryl or alkyl group (Devdatta, 2017). This azomethine compounds are more commonly called Schiff base courtesy of the fact that, Schiff Hugo a German, was the first scientist to identify the azomethine ligands in 1864 and so, these Lewis bases called ligands have been named after him (Suresh et al., 2015). These azomethines are thought to be versatile ligands due to their structural stability and synthetic flexibility and they are being carefully investigated and/or tested for their amazing pharmacological effects (Shabbir et al., 2017). Azomethine compounds and their metallic complexes possess a wide range of biological activities due to the presence of the -C=N- imine link (Wail et al., 2018). Due to their enhanced antibacterial, antifungal, antitumor, anticancer, antiradical, anti-tubercular, antimalarial, reactive oxygen species (ROS) scavenging, and antiviral activities, a number of azomethine chelators and their metallic complexes have drawn significant interest from medicinal chemists and biologists (Festus, 2017). These azomethine compounds' exceptional propensity to chelate with transition metals in particular has greatly increased their biological activities (Wail et al., 2018). Azomethines having oxygen and nitrogen donors have been reported to possess enhanced remarkable biological properties (Křikavovà et al., 2016). Also, the nitrogen atom in azomethines, provides binding

sites for metal ions; and makes attachment with various substrates of bio-molecules like proteins and amino acids in biological systems and that of diseases-causing germs possible (Habu, 2018). Through the metabolic activities, our body generates azomethine complexes that show activities against various microbes (Habu, 2018). Mild steel is a widely utilized alloy that is essential to several industries this is because of its chemical characteristics, mechanical strength, weldability, and machinability. However, procedures that utilizes sulphuric acid (H_2SO_4) and hydrochloric acid (HCl) such as acid-pickling, acid-cleaning, and acid descaling are employed in numerous sectors to prepare and clean the surface of steel products leads to the corrosion of the steel (Fahimeh et al., 2023). Interestingly, organic inhibitors are widely used and have been acknowledged as suitable options for reducing this harmful acid environment attack on metallic material. By using an adsorption mechanism on the metal surface, the organic inhibitors block the active sites by displacing water molecules and create a barrier layer that inhibits corrosion (Rezvani et al., 2020). Electrostatic interactions or a charge transfer from inhibitor molecules to the metal surface may be the cause of the adsorption of inhibitor compounds, which is regarded as a physical and chemical process respectively (Fahimeh et al., 2023). The effectiveness of the inhibition is dependent on the kind of environment, the heteroatoms present (such as oxygen, nitrogen, and sulfur), the nature of the substituent groups, electronic clouds, and the functional group present (Balildya et al., 2019). Interestingly, azomethine have gained popularity due to their enhanced protection capabilities, simple synthesis from comparably cheap starting materials, and environmental friendliness (Hosseinpoumajjar et al., 2022). These compounds, function as powerful inhibitors because their structures contain an imine (C=N) group. To examine the effectiveness of corrosion inhibitors, a variety of approaches have been employed (Abd Eli-Lateef et al., 2015). Numerous electrochemical methods are used to evaluate corrosion behavior based on electrochemical parameters, such as potentio-dynamic polarization (PDP) and electrochemical impedance spectroscopy (EIS). Additionally, the weight loss (WL) evaluation is a reliable method for assessing the inhibitor molecules' protective qualities. It is also a useful way to support the information discovered through electrochemical investigations (Murmu et al., 2019).

Materials and Methods

Materials: 2-hydroxyl-1-naphthaldehyde, 2-amino-6-nitrobenzothiazole, 2,2'-bipyridine, manganese (II) acetate tetrahydrate, iron(II)tetraoxosulphate(VI)heptahydrate, cobalt(II)chloridehexahydrate, nickel(II)acetatetetrahydrate, copper(II)acetatedihydrate, zinc(II)acetatedihydrate, distilled water (H_2O), acetic acid, triethylamine, ethanol(CH_3CH_2OH), chloroform, methanol, dichloromethane, acetone, hydrochloric acid, drying agent, DMF, and DMSO were used as received from the supplier (Bristol scientific).

Characterization: The melting/decomposition points of the chelator and its metal(II) complexes were obtained using a transparent cut-glass capillary tube in the electrochemical melting point machine. The infrared spectra of the compounds were recorded using a PerkinElmer Infrared Spectrophotometer in the region 4000–400 cm^{-1}. The Electronic reflectance spectra of all the complexes were recorded at room temperature using Perkin Elmer UV/Vis spectrometer from 900 to 190 nm

Corrosion studies: The corrosion inhibition study of the chelator was carried out using mild steel (ms) in acidic medium under different temperature (100 ^oC, 50 ^oC and 30 ^oC), time (1, 3, 6, 12, and 24 hours) and concentration (500, 300 and 100 ppm). The steels were bought from mile 3 market, cut into 4x4 dimension, abraded using emery papers, washed with soap solution, rinsed in H_2O, CH_3CH_2OH and acetone; and allowed to dry properly (Festus et al., 2020). Afterwards, the experiment was carried out using a thermostat water bath. The masses of the coupons before and after immersion were computed; and the weight loss, corrosion rate and percentage inhibition determined using;

$$\Delta W = \frac{m_1 - m_2}{A} \quad (1) \qquad CR = \frac{\Delta W}{t} \quad (2)$$

$$\Theta = \frac{CR_a - CR_p}{CR_a} \quad (3) \qquad \%IE = \Theta \times 100 \quad (4)$$

The results obtained from this study is summarized in Tables 4.1-4.5

Biological activity: Biological activity of the synthesized chelator and its metal(II) complexes were carried *in-vitro* by the agar diffusion technique using the microbes *Staphylococcus aureus, Bacillus cereus, Pseudomonas aeruginosa, Proteus mirabilis, Salmonella typhi* and *Klebsiella pneumoniae, Aspergillus niger, Aspergillus flaus,*

Cite this article as:
Festus, C., & Didia, L.E. (2023). Applied studies of heterocyclic substituted azomethine-based chelator and its divalent complexes: synthesis, spectral and theoretical characterization. *FNAS Journal of Scientific Innovations, 5*(1), 34-49.

and *Rhizopus stalonfer*. DMSO served as diluent for the various compounds as well as the negative control while miconazole and Streptomycin served as positive controls. A sterile cork borer of 8 mm was used to bore wells on the agar plates. In each well, 80 uL of the compound was added through the aid of a micro syringe, resulting into 80 µg per well. The inoculated plates were incubated at 37ºC for 18-24 h (bacteria) and 30ºC for 48 h (fungi) and the diameters (mm) of inhibition zones were measured. The antimicrobial tests were carried out in duplicates with mean activity determined (Olalekan & Didia, 2019). The results are recorded in Tables 4.6 and 4.7.

Synthesis of azomethine chelator and its M^{2+} complexes

Synthesis of HL^{31} chelator. About 7.0 g (4.07 x 10^{-2} mol) of 2-hydroxyl-1-naphthaldehyde was dissolved in 20 mL CH_3CH_2OH, stirred until homogeneous solution was obtained. Equivalent mole (4.07 x 10^{-2} mol) of 2-amino-6-nitrobenzothiazole was carefully introduced into the solution, followed by addition of 10 drops of acetic acid. The solution was left to reflux for about 6 h at 40 – 60 ºC. The yellow coloured product obtained had a mass of 9.014 g and a 77.66 %yield.

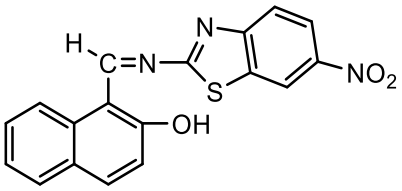

Proposed structure of azomethine chelator

Synthesis of metal(II) complexes. A 0.5 g (7.18 x 10^{-4} mol) HL^{31} dissolved in 20 mL CH_3CH_2OH, and stirred to acquire homogenous phase was differently reacted with $Mn(CO_2CH_3)_2.4H_2O$(0.176 g), $FeSO_4.7H_2O$(0.199 g), $Co(Cl_2).6H_2O$ (0.171 g), $Ni(CO_2CH_3)_2.4H_2O$ (0.179 g), $Cu(CO_2CH_3)_2.2H_2O$ (0.156 g) and $Zn(CO_2CH_3).2H_2O$ (0.158 g) in 10 mL on addition of 8 drops of triethylamine. Each resulting mixture was stirred and allowed to reflux for 6 h. The products were left to cool to room temperature, filtered, and dried. The masses and % yield obtained are as displayed in table 3.1.

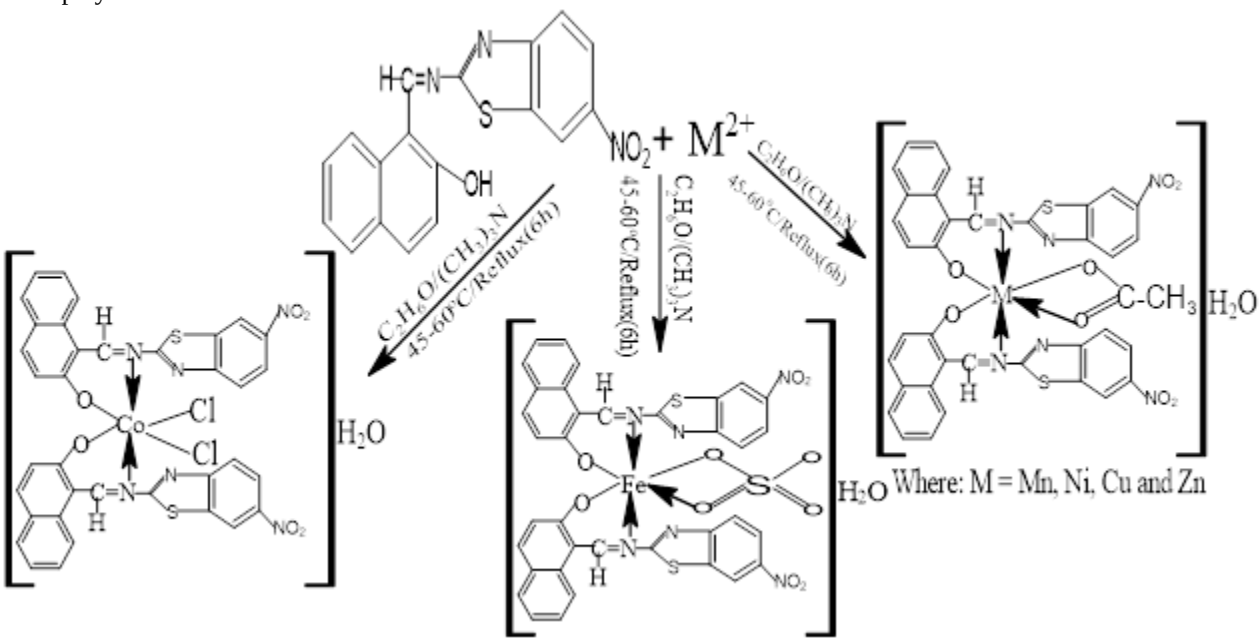

Scheme 2.2: Synthesis of M^{2+} complexes of azomethine based chelator

Results

Table 1. Analytical data for the chelator and its M^{2+} complexes

Compounds	Colour	M W (g/mol)	Yield(%)	M.Pt(°C)
$HL^{31}[C_{18}H_{11}O_3N_3S]$	Yellow	349.30	77.66	278 – 280
$[Mn(C_{38}H_{23}O_8N_6S_2]\ nH_2O$	Yellow	809.94	22.0	260 – 263
$[Fe(C_{36}H_{21}O_{10}N_6S_3]\ nH_2O$	pale yellow	847.85	88.4	> 360
$[Co(C_{36}H_{20}O_6N_6S_2Cl_2]\ nH_2O$	Brown	825.93	50.59	358 – 360
$[Ni(C_{38}H_{23}O_8N_6S_2]\ nH_2O$	orange	813.69	69.4	269 – 272
$[Cu(C_{38}H_{23}O_8N_6S_2]\ nH_2O$	Brick red	818.55	39.5	347 – 350
$[Zn(C_{38}H_{23}O_8N_6S_2]\ nH_2O$	Dirty green	838.41	22.1	> 360

The analytical data for the chelator and its M^{2+} complexes are presented in Table 1 above. From the Table, the chelator displayed yellow colour as well as the manganese complex while the iron complex had pale yellow colour. The cobalt, nickel, copper and zinc complexes had brown, orange, brick red and dirty green shades respectively. The chelator has a molar mass of 349.30 g/mol while the molar masses of the complexes ranged from 827.94 – 865.85 g/mol. The azomethine chelator (HL31) melted in the range 278 – 280 °C whereas its metal complexes all melted in the range 206 – 360 °C and above. The azomethine chelator as well as its complexes had percentage yields ranging from 39.5 - 88.4 %.

Solubility data for the chelator and its M^{2+} complexes. A solubility test of the azomethine chelator and the M^{2+} complexes was carried out in seven different solvents, at room temperature. The AC and a good number of M^{2+} complexes showed good solubility in DMSO and DMF (Yesmin et al., 2020), except for the Fe^{2+} complex that was insoluble, while Cu and Zn complexes were insoluble in DMF. All the M^{2+} compounds were generally insoluble in H_2O.

Table 2. Vibrational spectral results for the prepared chelator and its M^{2+} complexes

Compound	OH	C-H	C=N	C=C	C-N	C-C	NO_2	C-N	C-O	M-N	M-O
$HL^{31}\ [C_{18}H_{11}O_3N_3S]$	3401	2041	1633	1589	1515	1475	1331	1280	1122	–	–
$[Mn(C_{38}H_{25}O_9N_6S_2]nH2O$	3431	2082	1621	1600	1561	1436	1331	1276	1121	647	580
$[Fe(C_{36}H_{22}O_{11}N_6S_3]\ nH_2O$	3380	2351	1622	1600	1562	1436	1342	1276	1121	647	560
$[Co(C_{38}H_{25}O_9N_6S_2Cl_2]\ nH_2O$	3436	2082	1641	1613	1573	1424	1330	1250	1119	564	518
$[Ni(C_{38}H_{25}O_9N_6S_2]\ nH_2O$	3450	2074	1642	1591	1540	1435	1332	1250	1123	520	461
$[Cu(C_{36}H_{22}O_{11}N_6S_2]\ nH_2O$	3437	2164	1619	1602	1584	1428	1332	1253	1123	528	468
$[Zn(C_{38}H_{25}O_9N_6S_2]\ nH_2O$	3438	2347	1631	1587	1521	1455	1334	1231	1126	520	492

The infrared spectroscopic data of the compounds obtained from this study are as displayed in Table 2 above. The azomethine chelator and the metal complexes showed some functional groups and their vibrational bands as excepted for compounds of their structural type. The imine functional group (H-C=N) for the chelator appeared at 1633 cm^{-1} while those of the metal complexes appeared between 1616 – 1642 cm^{-1}. The hydroxy functional group (OH) of the chelator was seen at 3401 cm-1 while those of its metal complexes appeared between 3405 – 3450 cm^{-1}. The metal to donor atoms of the chelator bonding occurred between the metal to nitrogen (M-N) in the range 513 – 647 cm^{-1} and between the metal and oxygen (M-O) in the range 457 – 580 cm^{-1}.

Cite this article as:
Festus, C., & Didia, L.E. (2023). Applied studies of heterocyclic substituted azomethine-based chelator and its divalent complexes: synthesis, spectral and theoretical characterization. *FNAS Journal of Scientific Innovations, 5*(1), 34-49.

Table 3. Electronic spectra data for the prepared compounds

Compounds	Wavelength, λ_{max} (nm)	Absorption band, $\bar{\upsilon}$ (cm^{-1})	Transition(s)band assignment	Geometry
$[C_{18}H_{11}O_3N_3S]$	254, 308, 342	39370, 32468, 29239	$\pi \rightarrow \pi^*$, $n \rightarrow \pi^*$	
$[Mn(C_{38}H_{25}O_9N_6S_2]$	254, 352, 358	39370, 28409, 27933	$\pi \rightarrow \pi^*$, $n \rightarrow \pi^*$	
nH_2O	520, 640, 762	19231, 15625, 13123	d → d, d → d	Octahedral
$[Fe(C_{36}H_{22}O_{11}N_6S_3]$	314, 342, 400	31847, 29239, 25000	$\pi \rightarrow \pi^*$, $n \rightarrow \pi^*$	
nH_2O	648, 686	15432, 14577	d → d, d → d	Octahedral
$[Co(C_{38}H_{25}O_9N_6S_2Cl_2]$	300, 344, 352	33333, 29069, 28409	$\pi \rightarrow \pi^*$,$n \rightarrow \pi^*$	
nH_2O	622, 684	16077, 14619	d → d, d → d	Octahedral
$[Ni(C_{38}H_{25}O_9N_6S_2]$	302, 342, 398	33113,29239, 25126	$\pi \rightarrow \pi^*$, $n \rightarrow \pi^*$	
nH_2O	460, 634, 686	21739, 15773, 14577	d→d, d→d	Octahedral
$[Cu(C_{36}H_{22}O_{11}N_6S_2]$	262, 342, 358	38168, 33113, 29239	$\pi \rightarrow \pi^*$, $n \rightarrow \pi^*$	
nH_2O	648, 682, 762	15432, 14663,13123	d→d, d→d	Octahedral
$[Zn(C_{38}H_{25}O_9N_6S_2]$	254, 342, 398	39370, 32679, 25126	$\pi \rightarrow \pi^*$, $n \rightarrow \pi^*$	
nH_2O	652, 686	15337, 14577	d→d	Octahedral

The electronic spectra data of the synthesized compounds are as displayed in Table 3 above. The electronic data of the uncoordinated azomethine chelator, displayed four bands at 254, 308, 342 and 398 nm within the UV-region, which are due to transitions of the types л → л* and n → π* respectively. The metallic complexes under investigation also showed similar transitions but to somewhat slightly different range. In addition to the intraligand transitions, the metal (II) complexes showed absorption at visible in the range 428 – 822 nm assigned to d→d transitions with the exception of Zn without a d→d transition. The complexes were all assigned an octahedral geometry.

Applied studies: Corrosion inhibition study

Table 4.1. The study of the corrosion inhibition at 24 Hours/323 Kelvin

Compounds	Concentration	CR	% IE	Θ	ΔW
$HL^{31}[C_{18}H_{11}O_3N_3S]$	BLANK	3.021E-4	–	–	0.116
	100	1.2318E-4	59.23	0.5923	0.0473
	300	2.7604E-5	90.86	0.9086	0.0106
	500	1.758E-5	94.18	0.9418	0.00675

Table 4.2. The study of the corrosion inhibition at 12 Hours/323 Kelvin

Compounds	Concentration	CR	% IE	Θ	ΔW
$HL^{31}[C_{18}H_{11}O_3N_3S]$	BLANK	6.797E-4	–	–	0.1305
	100	2.094E-4	69.19	0.6919	0.0402
	300	1.235E-4	81.83	0.8183	0.02371
	500	3.0052E-5	95.58	0.9558	0.00577

Table 4.3. The study of the corrosion inhibition at 6 Hours/303 Kelvin

Compound	Concentration	CR	% IE	Θ	ΔW
$HL^{31}[C_{18}H_{11}O_3N_3S]$	BLANK	7.2167E-4	–	–	0.0866
	100	9.1666E-5	87.29	0.8729	0.011
	300	3.8333E-5	94.69	0.9469	0.0046
	500	3.5833E-5	95.03	0.9503	0.0043

Table 4.4. The study of the corrosion inhibition at 3 Hours and 373 Kelvin

Compounds	Concentration	CR	% IE	Θ	ΔW
HL^{31} [$C_{18}H_{11}O_3N_3S$]	BLANK	2.6354E-3	–	–	0.1265
	100	2.5063E-3	4.89	0.0489	0.1203
	300	7.3125E-4	72.25	0.7225	0.0351
	500	2.0052E-4	92.39	0.9239	0.0096

Table 4.5 The study of the corrosion inhibition at 1 Hours and 373 Kelvin

Compounds	Concentration	CR	% IE	Θ	ΔW
HL^{31} [$C_{18}H_{11}O_3N_3S$]	BLANK	7.225E-3	–	–	0.1156
	100	5.2125E-3	27.85	0.2785	0.0834
	300	2.05E-3	71.63	0.7163	0.0328
	500	4.6875E-4	93.51	0.9351	0.0075

The result obtained from the corrosion study of the azomethine chelator are as recorded in Tables 4.1 – 4.5. Three different concentrations were used to conduct the study, i.e., 100, 300 and 500 ppm. Three different temperature rates were also used, i.e., 303, 323 and 373 K while 6 different time intervals were studied, i.e., 1, 3, 6, 12 and 24 hours. The highest % inhibition efficiency (%IE) was recorded at 95.03 and that was for 6 h/303 K study while the least was recorded at 4.89 being 3 h/373 K study condition. The highest weight loss (weight loss) was found around 0.1305 for 12 h/323 K study while the least had a value of 0.0043 which was 6 h/303 K study condition.

Biological activity of the azomethine chelator, and its metal(II) complexes

Table 5.1. Antibacterial data of HL^{31} chelator and its M^{2+} complexes

Compounds	*B. c*	*K. p*	*P. a*	*P. m*	*S. a*	*S. t*
HL^{31} [$C_{18}H_{11}O_3N_3S$]	0.0 ± 0.0	6.5 ± 0.5	2.0 ± 0.0	8.0 ± 0.0	0.0 ± 0.0	6.0 ± 0.0
[$Mn(C_{38}H_{25}O_9N_6S_2]nH_2O$	7.5 ± 0.5	0.0 ± 0.0	2.0 ± 0.0	0.0 ± 0.0	13.0 ± 1.0	6.0 ± 0.0
[$Fe(C_{36}H_{22}O_{11}N_6S_3]nH_2O$	14.0 ± 0.0	0.0 ± 0.0	5.0 ± 1.0	6.0 ± 0.0	5.5 ± 0.5	5.0 ± 1.0
[$Co(C_{38}H_{25}O_9N_6S_2Cl_2]nH_2O$	0.0 ± 0.0	3.5 ± 0.5	0.0 ± 0.0	0.0 ± 0.0	7.0 ± 1.0	0.0 ± 0.0
[$Ni(C_{38}H_{25}O_9N_6S_2]nH_2O$	5.0 ± 1.0	1.0 ± 1.0	0.0 ± 0.0	5.0 ± 1.0	9.0 ± 1.0	4.0 ± 0.0
[$Cu(C_{36}H_{22}O_{11}N_6S_2]nH_2O$	10.0 ± 0.0	2.0 ± 0.0	6.5 ± 0.5	0.0 ± 0.0	12.0 ± 0.0	4.5 ± 0.5
[$Zn(C_{38}H_{25}O_9N_6S_2]nH_2O$	6.0 ± 0.0	4.5 ± 0.5	2.0 ± 0.0	0.0 ± 0.0	13.0 ± 1.0	6.0 ± 0.0
Streptomycin	18.0 ± 0.0	11.0 ± 1.0	9.0 ± 1.0	10.5 ± 0.5	19.0 ± 1.0	10.5 ± 0.5
DMSO	0.0 ± 0.0	0.0 ± 0.0	0.0 ± 0.0	0.0 ± 0.0	0.0 ± 0.0	0.0 ± 0.0

Table 5.1 above shows the antibacterial data of HL^{31} azomethine based chelator and its M^{2+} complexes. Six different bacterial strains were employed for this evaluation. The bacterial used are: *Staphylococcus aureus (S.a), Bacillus cerus (B.c), Pseudomonas aeruginosa (Ps.a), Proteus mirabilis (P. m), salmonella typhi (S. t)* and *Klebsiella pneumoniae (K. p).* Streptomycin was used as the standard drug, while DMSO was used as solvent control. The result presented activities in the range 1.0 – 14.0 mm for the metal complexes. The azomethine chelator had its activity in the range 2.0 – 8.0 mm. On the other hand, DMSO showed zero activity while streptomycin had good inhibitory impact on the test bacteria in the range 9.0 – 19.0 mm.

Table 5.2. Antifungi data of HL^{31} chelator and its M^{2+} complexes

Compounds	*A. n*	*A. f*	*R. s*
HL^{31} [$C_{18}H_{11}O_3N_3S$]	25.0 ± 1.0	21.0 ± 1.0	7.0 ± 1.0
[$Mn(C_{38}H_{25}O_9N_6S_2]nH_2O$	12.0 ± 0.0	11.5 ± 0.5	17.5 ± 0.5
[$Fe(C_{36}H_{22}O_{11}N_6S_3]nH_2O$	10.0 ± 0.0	6.0 ± 0.0	9.0 ± 1.0
[$Co(C_{38}H_{25}O_9N_6S_2Cl_2]nH_2O$	0.0 ± 0.0	0.0 ± 0.0	20.0 ± 0.0
[$Ni(C_{38}H_{25}O_9N_6S_2]nH_2O$	5.0 ± 1.0	7.0 ± 1.0	17.5 ± 0.5
[$Cu(C_{36}H_{22}O_{11}N_6S_2]nH_2O$	11.0 ± 1.0	0.0 ± 0.0	0.0 ± 0.0
[$Zn(C_{38}H_{25}O_9N_6S_2]nH_2O$	0.0 ± 0.0	1.0 ± 1.0	13.0 ± 1.0
Miconazole	17.0 ± 1.0	19.5 ± 0.5	16.0 ± 0.0
DMSO	0.0 ± 0.0	0.0 ± 0.0	0.0 ± 0.0

Cite this article as:
Festus, C., & Didia, L.E. (2023). Applied studies of heterocyclic substituted azomethine-based chelator and its divalent complexes: synthesis, spectral and theoretical characterization. *FNAS Journal of Scientific Innovations, 5*(1), 34-49.

Antifungi data of the azomethine based chelator and its M^{2+} complexes are presented in Table 5.2 above. Three different test organisms were used, namely: *Aspergillus niger (R.s), Aspergillus flaus (A.f),* and *Rhizopus stalonfer (R.s).* Miconazole served as the standard drug while DMSO was used for the dissolution of the compounds and as well served as solvent control. The inhibitions were recorded in the range 1.0–25.0 mm. The Mn^{2+} complex had the best activity for all the fungi, its mean inhibition values are 17.5, 12.0, and 11.5 mm against R.s, A.n, and A.f respectively. The azomethine based chelator also had significant inhibitory activity against all the test fungi (A.n (25.0 mm), A.f (21.0 mm) and R.s (7.0 mm)).

Discussion

Analytical study

The azomethine chelator as well as its complexes had good yields ranging from 39.5 – 88.4 %. From stoichiometric point of view, the azomethine chelator reacted with the metals in 2:1 molar ratio. The azomethine chelator (HL31) melted in the range 278 – 280 ºC whereas its metal complexes all melted in the range 206 – 360 ºC and above. No metal complex had the same melting point as the chelator confirming the formation of new compounds. Also, the different shades of colour assumed by the various compounds shows that new compounds indeed has been formed (Yesmin et al., 2020).

Fourier transition infrared (FT-IR) spectroscopic study

To identify potential coordination sites that could be involved in chelation, the spectra of the complexes and the free chelator were compared. Chelation is predicted to cause changes in the positions and/or intensities of these peaks, and the complexes' spectra showed evidence of this. Comparing the spectra obtained in this study with those reported in literature of similar systems, important bands were then tentatively assigned (Ahmed et al., 2015). In the spectrum of the chelator, the vibrational band characteristic of primary amine and carbonyl were not observed. This evidently show the formation of imine (H-C=N) functional group. The band observed at 1633 cm-1 for the AC, was shifted to entirely different frequencies within 1616 – 1642 cm-1 in the M2+complexes, this clearly indicates that azomethine nitrogen coordinated to metal ion (Hamil et al., 2020). The significant shift in these bands' positions in the metal complexes reveals the appearance of new bands in the 457–580 cm−1 and 513–647 cm−1 regions (Festus & Okocha, 2017). These bands are associated with the coordination complexes' M–O and M–N vibrations (Borase et al., 2021). The infrared spectrum of the AC shows a prominent absorption band at 3401 cm-1, which was attributed to the intramolecular H-bonding vibration (υO-H) of an enol tautomer. This reaction is typical of azomethine chelators with hydroxyl groups (Festus & Wodi, 2021). The hydroxyl group was deprotonated, and it is plausible that the AC also bonded with the metal ions through the deprotonated naphthol oxygen atom, as shown by the absence of the OH band in the spectra of the M2+ complexes. Despite the presence of a broad band in the complexes' spectra between 3380 and 3450 cm-1, Festus et al. (2023) identified this as the OH group of water molecules. Strong bands associated with the aromatic systems were present between 1559 and 1613 cm-1; and 1514 and 1584 cm-1 respectively, and are attributed to the C=C bending and C-N stretching vibrations. The C to NO2 bond was seen around 1330–1342 cm-1 (Elemike et al., 2018). The ν(phenolic C-O) band of the AC was detected around 1341 cm–1. However, the aforementioned band moved to 1116–1147 cm–1 in the metal complexes' spectra as a result of the hydroxyl oxygen's involvement in chelation. The (C-N) bands were seen in the 1231–1280 cm-1 range (Fasina et al., 2014).

Electronic spectroscopic study

In the Azomethine chelator, the bands observed between 254-398 nm were associated with these λ_{max} of л – л* for the aromatic ring and $n \rightarrow \pi^*$ conforming to intra-ligand charge transfer transitions. The latter affirms the participation of -C=N- group in coordination (Muhammad, 2018). These are due to the presence of lone pair of electrons on the heteroatom (N) and double bonds in C=C and C=N groups in the azomethine ligand structure (Dey et al., 2014). These transitions comprise the movement of electron from the non-bonding electron pair to the anti-bonding (л*) orbital within the compound (Fasina & Ogundele, 2014). When examining the spectra of every metal complex, it was found that in addition to the ligand's $\pi \rightarrow \pi^*$ and $n \rightarrow \pi^*$ transitions (though in somewhat different absorption band), they also showed bands above 400 nm (Ekennia et al., 2019).

The electronic reflectance spectra of the Mn^{2+} complex, $[Mn(C_{38}H_{23}O_8N_6S_2)]nH_2O$ displayed three distinct bands at 520, 640 and 762 nm due to $d \rightarrow d$ transitions for octahedral geometry (Hamil et al., 2020). The high energy bands

for this complex are observed at 254nm, and 352–358 nm assignable to $\pi\rightarrow\pi*$ and $n\rightarrow\pi*$ transitions (Xavier, & Srividhya, 2014). The iron complex, $[Fe(C_{36}H_{20}O_{10}N_6S_3)]nH_2O$ displayed two characteristic bands at 648 and 640 nm arising from $^5T_{2g} \rightarrow {}^5A_{1g}$, and $^5T_{2g}\rightarrow{}^5B_{1g}$ transitions typical of a spin-crossover within octahedral geometry (Festus et al., 2023). The high energy bands for this complex were observed at 314 and 342 nm, assignable to $\pi\rightarrow\pi*$ and $n\rightarrow\pi*$ transitions respectively. The cobalt complex, $[Co(C_{36}H_{20}O_6N_6S_2Cl_2)]nH_2O$ showed two different bands in high wavelength region of the spectrum at 400, 622 and 684 nm. The former band is assignable to $^3T_{1g} \rightarrow {}^3A_{2g}$, $^3T_{1g} \rightarrow {}^3T_{1g}$ and $^3T1_g \rightarrow {}^3T_{2g}$ transitions, confirming its octahedral coordination (Mahmoud et a., 2020). The high energy bands for this complex were observed at 300 and 344–352 nm, assignable to $\pi\rightarrow\pi*$ and $n\rightarrow\pi*$ transitions (Xavier, & Srividhya, 2014). The electronic spectrum of nickel complex $[Ni(C_{38}H_{23}O_8N_6S_2)]nH_2O$ showed three different bands at higher wavelength 460, 634 and 686 nm. These are d-d transitions assignable to $^3T_{1g}\rightarrow{}^3A_{2g}$, $^3T_{1g}\rightarrow{}^3T_{1g}$ and $^3T_{1g}\rightarrow{}^3T_{2g}$ octahedral transitions (Festus, 2021), along with the bands in the low wavelength region at 302 and 328 nm, attributed to $\pi\rightarrow\pi*$ and $n\rightarrow\pi*$ transitions, respectively (Kundu et al., 2016). The electronic absorption spectrum of the copper complex, $[Cu(C_{38}H_{23}O_8N_6S_2)]nH2O$ exhibited absorption band in the high wavelength region of 648 and 682 nm ascribed to $^2E_g\rightarrow{}^2T_{2g}$ transition suggestive of octahedral geometry (Narendra & Parashuram, 2017). Other high energy bands for the Cu^{2+} complex was observed at 262 and 358 nm for $\pi\rightarrow\pi*$ and $n\rightarrow\pi*$ LMCT transitions. The zinc complex, $[Zn(C_{38}H_{23}O_8N_6S_2)]nH_2O$ in its electronic spectrum displayed high energy absorption band at 254 nm associated with $\pi\rightarrow\pi*$ transition and 306 nm assignable to the LMCT, compatible with octahedral geometry (Festus et al., 2023).

Azomethine chelator and its impacts on acid corrosion of ms: The novel azomethine chelator was used to carry out a protective evaluation for mild steel in 1 mol/dm^3 HCl, using gravimetric method. The calculations of ms were carried out with and without the presence of the azomethine inhibitor at different concentration, time and temperature in a uniform solution. Tables 4.1 – 4.5 displays the weight lost (WL) for each concentration of the AC. According to the results obtained, total weight lost for 24 h was higher than that of 12 h in all concentrations except for 100 ppm; comparing the WL for 3 h to 1 h at the same concentrations and temperatures, that of 1 h was higher (this is contrary to what was envisaged since 3 h contact between the inhibitor and the ms provides longer interaction and possible coating of the surface and consequently inhibition should be more evident. This anomalous behaviour could be as a result of the DMF solvent used in the preparation of the 3 h test solution whereas the rest test solutions were all prepared using DMSO). The investigation carried out for 6 h had a significant weight loss higher than for those observed in 3 and 1 h even when the temperature for 6 h was lesser than those of 3 and 1 h. Generally, this decline in weight lost could be attributed to prolong exposure time and temperature leading to greater absorption of inhibitor, hence the concentration was the same. Also, from Table 4.1, corrosion rate (CR) decreased more in the inhibitor as compared to the blank and it even decreased more with higher concentrations of the inhibitor.

Tables 4.1 and 4.2, respectively, present the CR and % inhibition efficiency derived from weight lost findings in 24 h and 12 h. The results indicated that the chelator had good corrosion inhibition behavior in contrast to corrosion of ms in a 1 mol/dm^3 HCl solution. When utilizing various inhibitor concentrations in HCl, the AC showed greater ability to block the corrosion of the steel. Due to the steel's greater surface area and the presence of an inhibitor with a larger molecular weight, more inhibitor molecules were able to adsorb on the metal's surface. It followed that the azomethine chelator was spontaneously adsorbed on the mild steel (Zemede & Kumar, 2015). The presence of the functional groups C=N, NO_2, S, and OH in the azomethine chelator may also have aided and improved the chelator's ability to block ms and its corrosion, since ligands containing nitrogen and sulfur, have more electron pairs/polarizable electron clouds (John et al., 2017).

Resultant effect of altered concentrations of the azomethine chelator (inhibitor) at 24 – 1 h on total weight loss.

The total WL of ms at the different concentrations of the inhibitor at altered time and constant temperature are presented in Tables 4.1 – 4.5. From the results, the WL recorded are 0.116, 0.0473, 0.0106 and 0.00675 g (in 24 h) and 0.100, 0.0322, 0.007625, and 0.0046 g (at 12 h) of the inhibition respectively. The outcome indicated an apparent drop in CR or WL as the time reduces. The plot (Fig. 4.1ai) in appendix 4ai similarly revealed that total WL at 24 h was higher compared to WL observed at 12 h. The total WL at 308 K and altered concentrations also established that increase in concentration of the azomethine led to reduction in CR of the ms as shown in Table 4.5.

Cite this article as:
Festus, C., & Didia, L.E. (2023). Applied studies of heterocyclic substituted azomethine-based chelator and its divalent complexes: synthesis, spectral and theoretical characterization. *FNAS Journal of Scientific Innovations, 5*(1), 34-49.

Furthermore, when the inhibition studies carried out at the same temperature, 373 K but varied time (3 and 1 h) were compared, the outcome was to some extent consistent with what have been already observed in the previous cases for instance, the WL for 3 h (0.1265, 0.1203, 0.0351 and 0.0096) were higher than those recorded for 1 h (0.1156, 0.0834, 0.0328 and 0.0075). This affirms that prolong contact time between the inhibitor and the coupon enhances the performance of the chelator by increasing the weight lost (Festus & Wodi, 2022).

Inhibitor concentration and its influence on the rate of corrosion of ms.

The corrosion of ms in a mol/dm^3 HCl with and without the azomethine chelator at different concentrations, as represented by the graphs of CR vs IC (appendix 4). The figures demonstrated a decrease in CR when the inhibitor concentration rose at the same temperature and time as it did when the azomethine were present as opposed to when the acid solution was free of inhibitors. Figures 4.1aii-eii shows plots of inhibition efficacy against inhibitor concentration. The plots showed that as inhibitor concentration increased from 100 to 500 ppm, the effectiveness of inhibition increased as well. Inhibition efficiencies of 95.58%, 95.03% (94.69%), 94.18%, 93.51%, and 92.39% were detected at 12, 6, 24, 1, and 3 h, respectively. The availability of heteroatoms like N and S as well as functional groups like OH, NO_2, and C=N may be the primary cause of the inhibition achieved by the azomethine chelator. Additionally, this ability may be linked to the adsorption of inhibitor on the ms outer surface via the imine moiety's free electron pairs and π-electrons of the cyclic rings. This behavior indicates that the azomethine preventing the acid corrosion of the steel, possibly due to the phytochemical contents of the inhibitor adhering to the metallic surface. As the effectiveness of adsorption increases in a similar way, increasing inhibitor concentrations cause surface coverage to continuously expand (Silas et al., 2020). The pace at which the steel corroded reduced as inhibitor concentration rose. Higher ligand concentrations resulted in improved inhibitory efficiency. The mild steel surface was heavily covered with the inhibitor, which prevented reaction sites from being available. Hydrogen development was slowed down by the inhibition of metal disintegration as well. Consequently, corrosion was prevented from affecting the mild steels. Adsorption produces a homogeneous layer that inhibits the metal surface's contact with abrasive media, hence lowering corrosion (Nur et al., 2020).

Antibacterial assay of the azomethine based chelator and its metal(II) complexes

The synthesized chelator and its M(II) complexes were subjected to antibacterial screening in DMSO (which also served as negative control) against six bacterial strains (Staphylococcus aureus, Bacillus cereus, Pseudomonas aeruginosa, Proteus mirabilis, Salmonella typhi and Klebsiella pneumoniae) using streptomycin as positive control. The results obtained were summarized in Table 4.6. Results obtained from the antimicrobial screening indicated that the azomethine chelator and the complexes showed good activity against some of the bacterial strains in the range 1.0–14.0 mm. The Fe, Cu, Ni and Zn complexes were able to inhibit all the bacterial strains except Klebsiella pneumoniae, Proteus mirabilis, Pseudomonas aeruginosa, and Proteus mirabilis where they respectively showed zero activity. Mn complex had the next inhibitory potential, it inhibited all the bacterial strains except Klebsiella pneumoniae and Proteus mirabilis while Co complex had the least action as it only inhibited the growth of Staphylococcus aureus (7.0 mm) and Klebsiella pneumoniae (3.5 mm) but could not inhibit the growth of the other microorganisms. The standard drug, streptomycin had activity (9.0 – 19.0 mm) against all the bacterial strains and was found to have better inhibitory activity that most of the synthesized complexes and chelator. The chelator on its part, had moderate activity (2.0–8.0 mm) on all the test bacterial, except for Staphylococcus aureus and Bacillus cereus where there was no record of any activity. Interestingly, due to chelate effect, the metal complexes had improved activity than the chelator. The ability of these complexes in inhibiting the growth of these microorganisms is due to their structural similarities with natural biological compounds (Festus et al., 2020) and also due to presence of the imine (-N=CH-) active pharmacophore, which play major roles in their significant bio-activities (Habu, 2018). The metal(II) complexes have the presence oxygen and nitrogen and these have been reported to possess a wide remarkable biological activity (Křikavovà et al., 2016). The presence of the metal ions in the complexes also enhanced their performance in bacterial inhibition (Habu, 2018).

Antifungi study of the chelator and its M(II) complexes

The data obtained from this assay are summarized in Table 4.7. From the result, the least activity had a mean value of 1.0 mm while the highest activity was recorded at mean value of 25.0 mm. The chelator had significant inhibitory activity against all the test fungi (*Aspergillus niger* (25.0 mm), *Aspergillus flaus* (21.0 mm) and *Rhizopus stalonfer* (7.0 mm)) thereby presenting it as a promising antifungi pro-drug agent. Amongst the complexes, Mn^{2+} complex had the best of activities for all the fungi, its mean inhibition values include 17.5, 12.0, and 11.5 mm against *Rhizopus*

Cite this article as:
Festus, C., & Didia, L.E. (2023). Applied studies of heterocyclic substituted azomethine-based chelator and its divalent complexes: synthesis, spectral and theoretical characterization. *FNAS Journal of Scientific Innovations, 5*(1), 34-49.

stalonfer, Aspergillus niger, and Aspergillus flaus respectively. All the complexes with the exception of Cu^{2+} complex inhibited *Rhizopus stalonfer* fungus. Similarly, *Aspergillus fungus* was inhibited by almost all the complexes except Co^{2+} and Cu^{2+} complexes that did not show any activity while the *Aspergillus niger* fungus was inhibited by most of the complexes excluding the Co^{2+} and Zn^{2+} complexes. When compared with the standard drug (miconazole), some of the novel metal complexes such as Mn^{2+}, Co^{2+} and Ni^{2+} were found to be better inhibitors against *Rhizopus stalonfer*, while for *Aspergillus niger, and Aspergillus flaus* fungal the miconazole was found to be better inhibitor. The negative control, DMSO showed zero activity to the fungi used for this study. The activity of the complexes can be explained on the basis of Overtones concept and Tweedy's chelation theory (Yesmin et al., 2020). Also, several reports on the antimicrobial activity of metal complexed azomethine based ligands have presented them as more promising inhibitors with improved bio-functions (Habu, 2018).

Conclusion

A novel azomethine chelator (HL^{31}) was synthesized from the reaction of 2-amino-6-nitrobenzothiazole with 2-hydroxy-1-naphthaldehyde. The M^{2+} complexes were prepared from 2:1 stoichiometric reaction of the chelator and metal salts respectively. The analytical and spectral data obtained were used to characterize the azomethine chelator and the complexes in order to ascertain the composition and properties of the compounds. Via the FT-IR data it was confirmed that coordination between the AC and the metal ions actually occurred and this coordination occurred between the metal and nitrogen (M-N) as well as between the metal and oxygen group in the chelator (M=N). The electronic spectra suggested the proposed geometries for the complexes. The corrosion study proved the azomethine chelator as good inhibitory agent. Also, the antimicrobial screening revealed that the azomethine chelator and its M^{2+} complexes had significant antifungal and antibacterial activities and so, they could be promising antibacterial and antifungi agents.

References

Abd El-Lateef, H. M., Abu-Dief, A. M., Abdel-Rahman, L. H., Sañudo, E. C. & Aliaga-Alcalde, N. (2015). Electrochemical and theoretical quantum approaches on the inhibition of C1018 carbon steel corrosion in acidic medium containing chloride using some newly synthesized phenolic Schiff bases compounds. *Journal of Electroanalytical Chemistry, 2015*(743), 120–133. Doi: 10.1016/j.jelechem.2015.02.023.

Ahmed, N., Riaz, M., Ahmed, A. & Bhagat, M., (2015). Synthesis, characterisation, and biological evaluation of Zn(II) complex with tridentate (NNO Donor) Schiff base ligand. *International Journal of Inorganic Chemistry*. ID 607178, doi:10.1155/2015/607178.

Aliyu, H. N. & Zayyan, R. S. (2014). Synthesis, Analysis and Bioactivity Evaluation of Copper(II) Tetradentate Schiff Base Complex. *International Journal of Current Microbiology and Applied Science, 3*(1), 445-452.

Baildya, N., Ghosh, N. N. & Chattopadhyay, A.P. (2019). Anti-corrosive properties of quercetin and its derivatives on Fe(111) surface: a quantum chemical approach. *Applied. Science*, **1**, 735. https://doi.org/10.1007/s42452-019-0772-1

Borase, J. N., Mahale, R. G., Rajput, S. S. & Shirsath, D. S. (2021). Design, synthesis and biological evaluation of heterocyclic methyl substituted pyridine Schif base transition metal complexes. *A springer nature journal, 3*(197).

Devdatta, V. S., Prafullkumar, A. K., Deshpande, V. G. & Seema, I. H. (2017). Heterocyclic Schiff base Cu(II) metal complexes and their X-Ray diffraction study, *European J of Pharm Med Res, 4(9),* 680-683.

Dey, D., Ray, R. & Hazra, B. (2014). Antitubercular and antibacterial activity of quinonoid natural products against multi-drug resistant clinical isolates. Phototherapy Research, 28,1014-1021.

Ekennia, A. C., Onwudiwe, D. C., Osowole, A. A., Okpareke, O. C., Olubiyi, O. O. & Lane, J. R. (2019). Coordination compounds of heterocyclic bases: synthesis, characterization, computational and biological studies. *Res. Chem. Intermed. 45(3)*, 1169–1205.

Elemike, E. E., Nwankwo, H. U., & Onwudiwe, D. C. (2018). Synthesis and characterization of Schiff bases NBBA, MNBA and CNBA. Elsevier.) e00670. doi: 10.1016/j.heliyon.2018.

Fahimeh, A., Ghomi, E. R., Dinari, M., & Ramakrishna, S. (2023). Recent Advances on the Corrosion Inhibition Behavior of Schiff base Compounds on Mild Steel in Acidic Media. *Journal.chemistryeurope.org-ChemistrySelect, 8,* 1-31. Doi.org/10.1002/slct.202203231

Fasina, T. M. & Ogundele, O. (2014). Synthesis, characterization and antimicrobial activity of some transition metal complexes of schiff base derived from ophenylenediamine and 5 -nitrosalicyaldehyde. *Der Pharma Chemica, 6*(4), 18-22.

Fasina, T. M., Ogundele, O., Ejiah, F. N. & Dueke-Eze, C. U. (2014). Biological activity of copper(II), Cobalt(II), and Nickel(II) complexes of Schiff base derived from o phenylenediamine and 5-bromosalicylaldehyde. *International Journal of Biological Chemistry* vol 6 (1): 24-30.

Festus, C. (2017). Synthesis, characterization and antibacterial studies of heteroleptic Co(II), Ni(II), Cu(II) and Zn(II) complexes of N-(2-hydroxybenzylidene)pyrazine-2-carboxamide. *Int.l Journal of Chemistry, Pharmacy & Technology, 2*(5), 202-211.

Festus, C., & Okocha, O. (2017). Behaviour of *N*-(2-hydroxybenzylidene)pyrazine-2-carboxamide in complexation towards Fe(II), Co(II), Ni(II) and Cu(II) ions: Synthesis, spectral characterization, magnetic and antimicrobial properties. *International Journal of Chemistry, Pharmacy & Technology*, *2*(4), 143-153

Festus, C., Odozi, W. N., & Olakunle, M. (2020). Preparation, spectral characterization and corrosion inhibition studies of (*e*)-*n*-{(thiophene-2-yl)methylene}pyrazine-2-carboxamide Schiff base ligand. *Protection of Metals and Physical Chemistry of Surfaces, 56*(3), 651–662.

Festus, C., Ekpete, O. A., & Don-Lawson, C. D. (2020). Novel metal^{2+} complexes of *N*-(1,4-dihydro-1,4-oxonaphthalen-3-yl)pyrazine-2-carboxamide: Synthesis, structural characterization, magnetic properties and antimicrobial activities. *Current Research in Chemistry, 12*, 1-10.

Festus, C., Jude, A. I. & Collins, U. I. (2021). Ligation actions of 2-(3-hydroxypyridin-2-ylamino)naphthalen-1,4-dione: synthesis, characterization, In-vitro antimicrobial screening, and computational studies. *Indian, Journal Heterocyclic Chemistry, 31,* 1–13.

Festus, C., & Wodi, C. T. (2021). Corrosion inhibition; and antimicrobial studies of bivalent complexes of 1-(((5-ethoxybenzo[d]thiazol-2-yl)imino)methyl)naphthalene-2-ol chelator: Design, synthesis, and experimental characterizations. *Direct Research Journal of Chemistry and Materials Science, 8*(2021), 31-43.

Festus, C., Wodi, C.T. & Iyo, I. A. (2023). Performance of Organic Frameworks as Thriving Mild Steel Corrosion Inhibitors in Acid Medium: Syntheses and Characterization. *Protection of Metals and Physical Chemistry of Surfaces, 22*(4), 152.

Festus C., Ezugwu, C. & Okpareke, O. (2023). Synthesis, characterization, DFT and biological studies of Fe(II), Cu(II), and Zn(II) complexes of keto-imine chelators. *Inorganica Chimica Acta*., *545*, 3-9.

Habu, N. A. (2018). Schiff Bases and their Transition Metal Complexes: The Drugs for the Next Generation. Professorial Inaugural Lecture No. 3.

Hamil, A., Khalifa, M. K., Almutaleb, A. A., & Qasim, M. (2020). Synthesis, Characterization and Antibacterial Activity Studies of Some Transition Metal Chelates of Mn(II), Ni(II) and Cu(II) with Schiff Base Derived from Diacetylmonoxime with Ophenylenediamine. *Advanced Journal of Chemistry-Section A, 3*(4), 524–533.

Hosseinpournajjar, E, Kianfar, A H, & Dinari, M (2022). Synthesizing and characterization of Cu(II) polymer complex: application for removing heavy metals from aqueous solutions. *Journal of the Iranian Chemical Society, 19*(5), 1963–1977.

John, S., Jeevana, R., Aravindakshan, K. K. & Joseph, A. (2017). "Corrosion inhibition of mild steel by N(4)-Substituted thiosemicarbazone in hydrochloric acid media," *Egyptian, Journal of Petroleum, 26*(2), 405-412.

Krikavova, R., Vanco, J., Travnicek, Z., Buchtik, R. & Dvorak, Z. (2016). Copper(II) quinolinonato-7 carboxamido complexes as potent antitumor agents with broad spectra and selective effects. *Royal society of Chemistry advances, 5*(6), 3899-3909.

Kundu, S., Pramanik, A. K., Mondal, A. S., & Mondal, T. K. (2016). "Ni(II) and Pd(II) complexes with new N, O donor thiophene appended Schiff base ligand: Synthesis, electrochemistry, X-ray structure and DFT calculation." *Journal of Molecular Structure, 11*(16), 1–8.

Mahmoud, W. A., Hassan, Z. M. & Ali, R. W. (2020). Synthesis and spectral analysis of some metal complexes with mixed Schiff base ligands 1-[2-(2- hydroxybenzylideneamino)ethyl]pyrrolidine-2,5-dione (HL1) and (2 hydroxybenzalidine)glycine (HL2). *Journal of Physics: conference series*, 1660 012027. doi:10.1088/1742-6596/1660/1/012027

Muhammad, S. S., Muhammadu, M. Y. & Usman, S. U. (2018). Synthesis and evaluation of the efficacies of some schiff bases for the removal of heavy metals from wastewater. *Science World Journal, 13*(4), 108-114.

Murmu, M., Saha, S. K., & Murmu, N. C., & Banerjee, P. (2019). Effect of stereochemical conformation into the corrosion inhibitive behaviour of double azomethine based Schiff bases on mild steel surface in 1 mol/L HCl medium: An experimental, density functional theory and molecular dynamics simulation study**.** *Corrosion Science, 146,* 134-151.

Narendra, K. C., & Parashuram, M. (2017). Metal Complexes of a Novel Schiff Base Based on Penicillin: Characterization, Molecular Modeling, and Antibacterial Activity Study." *Bioinorganic Chemistry and Applications, 2017,* 1-13. https://doi.org/10.1155/2017/6927675

Nur, H., Abu, H., Nur, N., Mohd Zulkamal, P., & Nur, N. D. (2020). Schiff Base as A Corrosion Inhibitor. Jasin 58-61.

Olalekan, T. E. & Didia, L. E. (2019). Synthesis, characterization and antimicrobial activity of o-phenylenediamine Schiff base and its metal(II) complexes. *Science Focus, 23*(1), 1–10. DOI:10.36293/sfj.2019.0032.

Rezvani, M., Rahmanzadeh, A. & Ganji, D. M. (2023). Corrosion protection performance of Laurhydrazide N' propan-3-one (LHP) adsorbed on zinc surface: A DFT-MD simulation investigation. Materials Today Communications, 36. https://doi.org/10.1016/j.mtcomm.2023.10646.

Samaszko-Fiertek, J., Raczuk, E., Dmochowska, B., & Madaj, J. (2022). Different Schiff Bases Structure, Importance and Classification. *Molecules, 27*(3), 787.

Silas, O., Ejiroghene, K.O., & Rogers, T. (2020). Corrosion evaluation on mild steel in different selected media. *International Journal of Engineering Applied Sciences and Technology, 5*(3), 33-38.

Suresh, R., Sakthinathan, S. P., Kamalakkannan, D., Ranganathan, K. Sathiyamoorthi, K., Mala, V., Arulkumaran, R. Vijayakumar, S., Sundararajan, R., Vanangamudi, G., Subramanian, M., Thirunarayanan, G., Vanaja, G., & Kanagambal, P. (2015). Solvent-Free Synthesis of Azomethines, Spectral Correlations and Antimicrobial Activities of Some E-Benzylidene 4-Chlorobenzenamines. *Bulletin of Chemical Society of Ethiopia., 29*(2), 275-290.

Wail., Al-Hamdani, A., Ahmed, S., Basheer, H., Al-Luhaibi, R., Dib, A. & Ko, Y. (2018). Synthesis, characterization, and antioxidant activities of imine compounds. *Journal of Physical Organic Chemistry 32*(1). DOI:10.1002/poc.3916

Xavier, A. & Srividhya, N. (2014). Synthesis and Study of Schiff base Ligands. *Journal of Applied Chemistry (IOSR-JAC), 7*(11), 06-15.

Yesmin, M. F., Hossain, M. S., Nasira, Uddin, N., Ashrafuzzaman, M. D., Haque, M. & Banu, L. A. (2020). Cu (II) and Ni (II) Complexes of Schiff Base: Synthesis, Characterization and Antibacterial Activity. *International Journal of Advanced Research in Chemical Science, 7*(1), 9-15.

Zemede, Y. B., & Kumar, A. S. (2015). "Synthesis, characterization, corrosion inhibition and biological evaluation of schiff bases. *International Journal of Chemical Technology Research, 7*(01), 279-286.

Appendix 1. IR Spectra

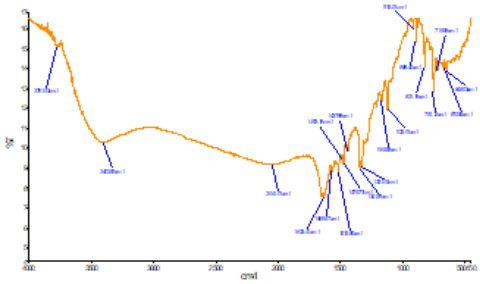

HL^{31}

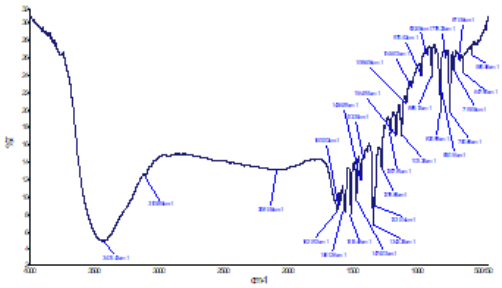

$[Mn(HL^{31})_2]$

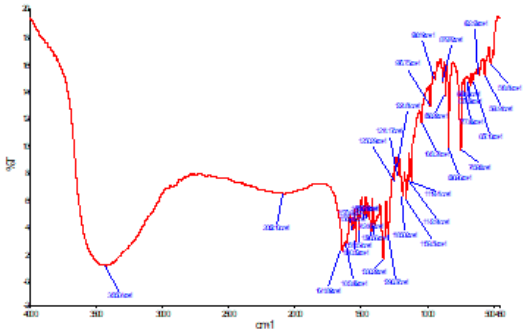

$[Fe(HL^{31})_2]$

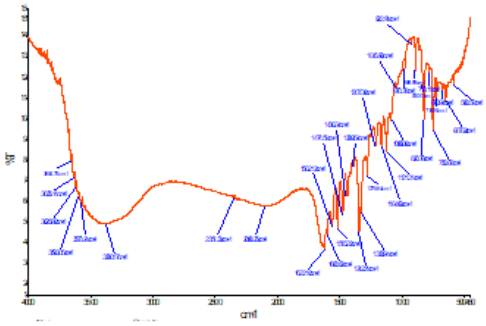

$[Co(HL^{31})_2]$

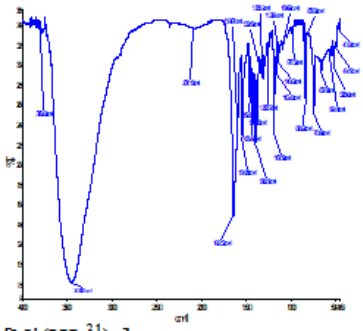

$[Ni(HL^{31})_2]$

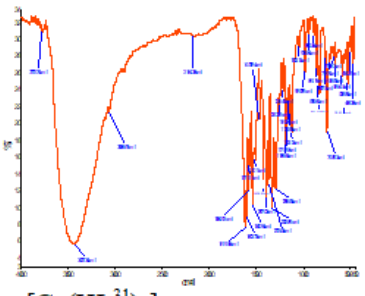

$[Cu(HL^{31})_2]$

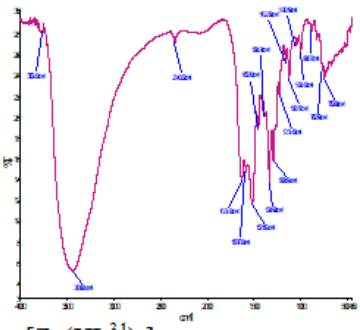

$[Zn(HL^{31})_2]$

Appendix 2. UV-VIS Spectra

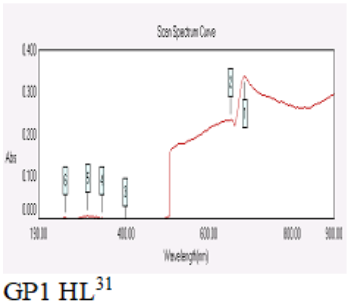

GP1 HL^{31}

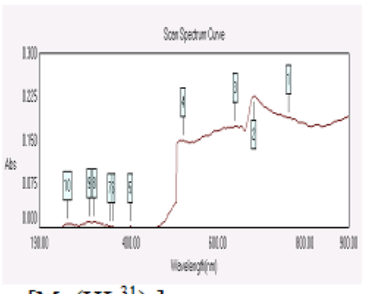

$[Mn(HL^{31})_2]$

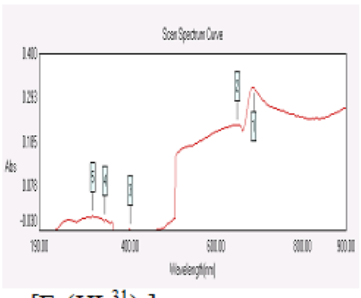

$[Fe(HL^{31})_2]$

Cite this article as:
Festus, C., & Didia, L.E. (2023). Applied studies of heterocyclic substituted azomethine-based chelator and its divalent complexes: synthesis, spectral and theoretical characterization. *FNAS Journal of Scientific Innovations*, *5*(1), 34-49.

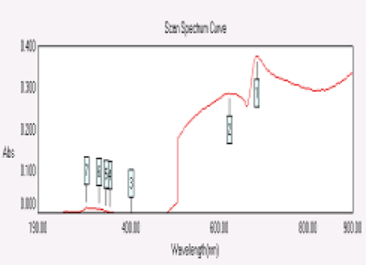

$[Co(HL^{31})_2]$

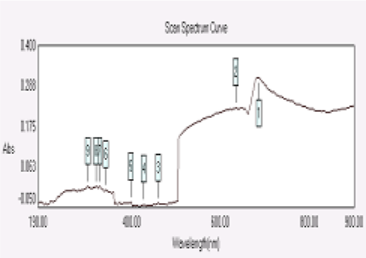

$[Ni(HL^{31})_2]$

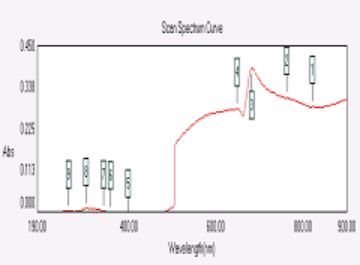

$[Cu(HL^{31})_2]$

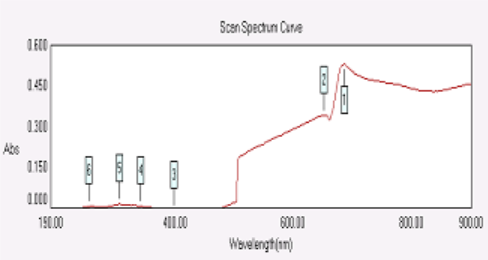

$[Zn(HL^{31})_2]$

Appendix 3. Corrosion inhibition graph of the azomethine based chelator

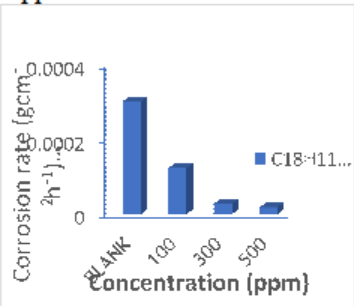

Fig. 4ai: Corrosion inhibition at 24h/323K

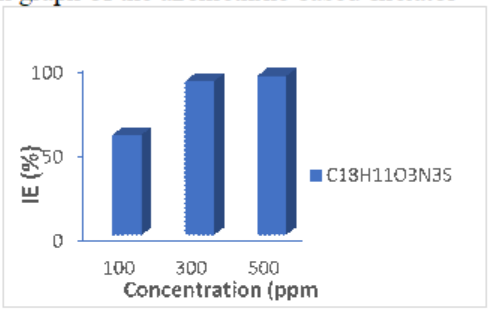

Fig. 4aii: Corrosion inhibition at 24h/323K

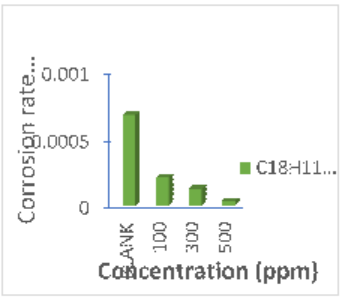

Fig. 4bi: Corrosion inhibition at 12h/323K

Cite this article as:
Festus, C., & Didia, L.E. (2023). Applied studies of heterocyclic substituted azomethine-based chelator and its divalent complexes: synthesis, spectral and theoretical characterization. *FNAS Journal of Scientific Innovations*, 5(1), 34-49.

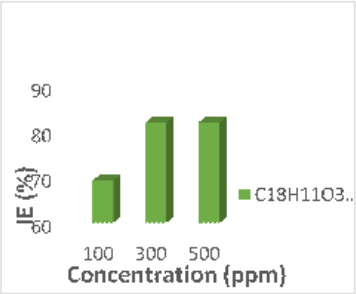

Fig. 4bi: Corrosion inhibition at 12h/323K

Fig. 4bii: Corrosion inhibition at 12h/323K

Fig. 4ci: Corrosion inhibition at 6h/303K

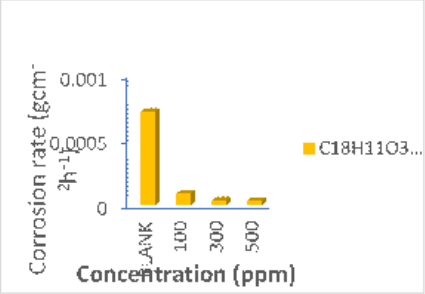

Fig. 4cii: Corrosion inhibition at 6h/303K

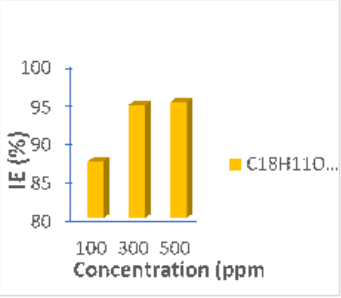

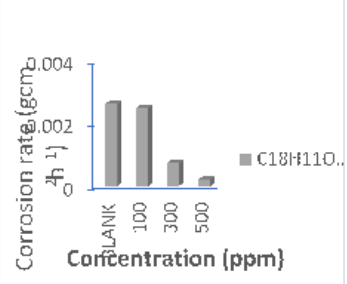

Fig. 4di: Corrosion inhibition at 3h/373K

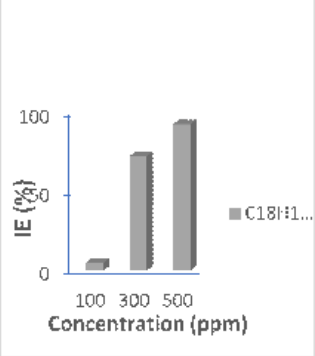

Fig. 4dii: Corrosion inhibition at 3h/373K

Cite this article as:
Festus, C., & Didia, L.E. (2023). Applied studies of heterocyclic substituted azomethine-based chelator and its divalent complexes: synthesis, spectral and theoretical characterization. *FNAS Journal of Scientific Innovations*, 5(1), 34-49.

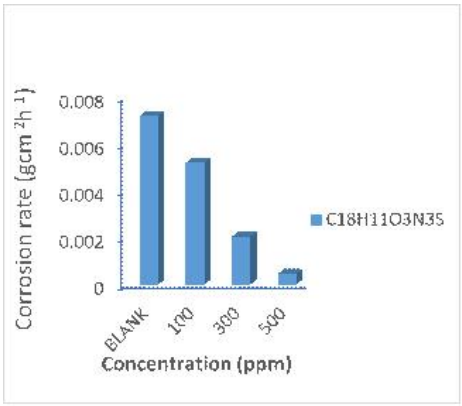

Figure 4ei: The study of the corrosion inhibition at 1 Hours/303 Kelvin

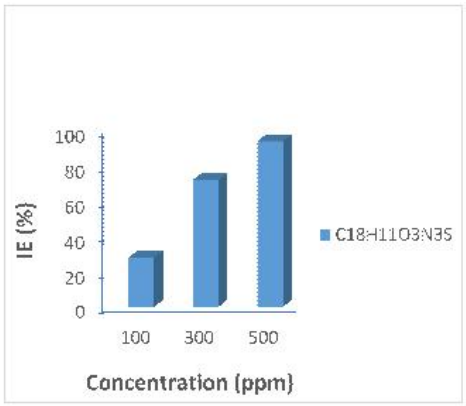

Figure 4ei: The study of the corrosion inhibition at 6 Hours/303 Kelvin

Appendix 5. Plates of antimicrobial assay of the azomethine based chelator and its M^{2+} complexes